More profound impact of CP ENSO on Australian spring rainfall in recent decades

Yiling Ma[1,2,3] · Jilin Sun[4] · Tianyun Dong[1,2,3] · Weidong Yu[1,2,3] · Wenjie Dong[1,2,3]

Abstract

Most of Australia was in severe drought from 2018 to early 2020. Here we link this drought to the Pacific and Indian Ocean sea surface temperature (SST) modes associated with Central Pacific (CP) El Niño–Southern Oscillation (ENSO) and Indian Ocean Dipole (IOD). Over the last 20 years, the occurrence frequency of CP El Niño has increased. This study extends the previous understanding of eastern Pacific (EP) El Niño-Australian rainfall teleconnections, exhibiting that CP El Niño can bring much broader and stronger rainfall deficiencies than EP El Niño during austral spring (September–November) over the northern Australia (NAU), central inland Australia and eastern Australia (EAU). The correlations between SST fields and rainfall in three Cluster regions divided by clustering analysis also confirm this, with rainfall variability in most of Australia except southern Australia (SAU) most significantly driven by CP ENSO. Also, we demonstrate that the CP El Niño affects rainfall in extratropical EAU via the Pacific-South American (PSA) pattern. While the influence of EP El Niño is only confined in tropical NAU because its PSA pattern sits far too east to convey its variability. With the development of ENSO diversity since 2000, the footprint of El Niño on Australian rainfall has become more complex.

Keywords Australian rainfall · ENSO diversity · IOD · Pacific-South American pattern

1 Introduction

Agriculture has historically been one of the most significant industries in Australia, both in terms of its domestic production as well as the export income. Agriculture and its closely related industries earn an average of $155 billion per year for a 12% share of Australia's total gross domestic product (GDP) (http://www.nff.org.au/farm-facts.html). Nevertheless, fluctuations in the gross value of Australian crops vary greatly from year to year (Nicholls 1985). If such

✉ Weidong Yu
  yuwd@mail.sysu.edu.cn

✉ Wenjie Dong
  dongwj3@mail.sysu.edu.cn

1 School of Atmospheric Sciences, Sun Yat-Sen University, Zhuhai 519082, China

2 Key Laboratory of Tropical Atmosphere-Ocean System, Ministry of Education, Zhuhai 519082, China

3 Southern Marine Science and Engineering Guangdong Laboratory, Zhuhai 519082, China

4 College of Oceanic and Atmospheric Sciences, Ocean University of China, Qingdao 266100, China

fluctuations are accurately predicted, there is a potential for huge savings and profits. Numerous studies have shown that, the interannual variability of crop production is mainly driven by climate factors, particularly precipitation and surface temperature, in the wheat growing seasons from May to November (Nicholls 1985; Yuan and Yamagata 2015). Therefore, understanding and developing a forecasting skill of Australian spring (September–November) rainfall is conducive to predicting and managing the production of crop in Australia. Furthermore, southwestern, southeastern and eastern Australia (EAU—the region of southern Queensland and New South Wales, located in the subtropics) have experienced substantial declines in cool season rainfall in recent decades (http://www.bom.gov.au/climate/change/). Part of Australia, especially southern Australia (SAU) has been suffering from drought with increasing severity and frequency (IPCC 2021, Chapter 11, Table 11.15). For example, the recent 2018-early 2020 drought had a severe damage on natural system and human lives for large parts of Australia, especially for the southern inland Queensland and inland New South Wales (BoM 2020). According to BoM (2020), 2018–2019 recorded the lowest two-year rainfall totals for the Murray Darling Basin (MDB). MDB is a vital

agricultural region known as the "food bowl" of Australia, and drought in this region thus has a severe impact on the regional and national economy. This prolonged drought dragged Australian real GDP to more than 0.7% below base, as well as a national welfare loss of $63 billion in 2018–2019 (Wittwer and Waschik 2021). Whilst unprecedented bushfires partially due to the drought swept across Australia from July 2019 to February 2020, which had a massive damage over a large part of Australia in many aspects including burning more than 17 million hectares of land, taking away thirty-three human lives and billions of animal lives (BoM 2020; Wittwer and Waschik 2021).

Recent research has shown that, some remote climate drivers contribute to the Australian drought in 2018–2019 (BoM 2020; King et al. 2020; Wang and Cai 2020; Watterson 2020). On the synoptic timescale, the shift of rain-bearing weather systems play an important role in generating this drought. On the intraseasonal-interannual timescale, the rainfall deficits during 2018–2019 have been shown to occur under the combined effects of the subtropical high-pressure ridge (BoM 2020), the sudden stratosphere warming (Lim et al. 2021a), the Southern Annular Mode (SAM) (Lim et al. 2021a), the Indian Ocean subtropical dipole (Ramsay et al. 2017), the El Niño–Southern Oscillation (ENSO) and Indian Ocean Dipole (IOD) (Watterson 2020; BoM 2020). The SAM occurred in the late spring of 2019 in a strong negative phase, which moderately exacerbated the dry conditions over subtropical EAU, attributed for 22% of the All-Australia 2019 springtime rainfall deficit (Watterson 2020). This SAM is shown to be induced by a strong Southern Hemisphere stratospheric warming associated with a weakened stratospheric circumpolar westerly jet occurred in the spring 2019 (Lim et al. 2021a). The tropical Indo-Pacific SST drivers also significantly account for the two-year rainfall deficits. For example, Watterson (2020) quantified the contribution of tropical Indo-Pacific SST variability on the 2018–2019 Australian rainfall deficit with a Pacific-Indian dipole (PID) index combining the west Pacific and east Indian influences. He argued that the PID index can explain 38% of the two-year deficit, and 54% of the SON 2019 deficit, indicating an important role of the tropical Indo-Pacific SST in this drought episode. Accordingly, as the major source of the tropical Indo-Pacific SST interannual variability (Ashok et al. 2003; Risbey et al. 2009; Ummenhofer et al. 2009), the ENSO and IOD are the main drivers for the interannual variability of Australian rainfall (Lim and Hendon 2015; Watterson 2020). Furthermore, the ENSO and IOD have a strong correlation with each other in austral spring (Risbey et al. 2009), and their combined effect on Australian rainfall is the strongest during this season (Watterson 2020). This is reasonable since they are both characterized by phase lock. Specifically, an IOD event typically peaks in austral spring. Though typically ENSO is still in its developing phase

during austral spring, it already has a comparable intensity and is strong enough to impact Australian rainfall (Lim et al. 2017). Therefore, when studying the individual impact of ENSO/IOD on Australian springtime rainfall, it is necessary to separate their covariant fraction. For instance, Cai et al. (2011) have shown that the IOD influences the rainfall over northern Australia (NAU) and EAU, while after removing the covariance with ENSO, IOD can only impact the southern Australian precipitation. Investigating the links of ENSO and IOD to regional rainfall variability is of great value for exploring potential predictability of Australian rainfall, because dynamical models still have limited skill in forecasting the spatial distribution of Australian rainfall especially in austral spring (Watterson et al. 2021). By evaluating the simulations of Climate Analysis Forecast Ensemble (CAFE), Watterson et al. (2021) argued that the predictive skill for All-Australia seasonal precipitation is largely consistent with skill for Indo-Pacific SST climate drivers, both with moderate correlations during austral spring and summer. This indicates that, the links of large-scale climate drivers (such as ENSO and IOD) to rainfall provide the foundation for skillful prediction of Australian spring rainfall (Lim et al. 2021b; Watterson et al. 2021).

So far, the traditional El Niño episode (referred to as EP El Niño in this article, with the strongest SSTA appearing in the equatorial eastern Pacific) has been well understood, including its operating mechanism and relationship with Australian rainfall for long-lead predictability (Risbey et al. 2009; King et al. 2014, 2020; Lim et al. 2017). Generally, this impact of EP ENSO on Australian spring rainfall can be divided into two parts: the tropical and the extratropical one. In the tropics, Australian rainfall is directly influenced by the ENSO through the western pole (around 120°E) of the Southern Oscillation (SO). SO is the atmospheric component of the ENSO characterized by an anomalous surface pressure "seesaw" between the tropical eastern Pacific and the Maritime Continent. During El Niño, sustained warming (cooling) occurs over the central and eastern tropical Pacific (Maritime Continent). As a response to the diabatic heating (cooling), an anomalous low (high) surface pressure appears in the lower-layer troposphere of the warming (cooling) area, associated with an (a) upward (downward) motion and an increase (reduction) in rainfall over the same area. Because of the Coriolis force, the deep baroclinic part of the SO is confined in the tropics. Therefore, during El Niño, rainfall is blocked in near-tropical Australia which is dominated by subsidence and anomalous high surface pressure, and vice versa for La Niña (McIntosh and Hendon 2018). The extratropical part, on the other hand, is argued to be influenced by El Niño via equivalent barotropic Rossby wave train response (Cai et al. 2011). During austral spring, ENSO conducts its impacts on SAU via the Rossby wave trains associated with IOD because of their strong covariation in

this season. In fact, the Rossby wave trains also exist during pure IOD in SON (Mclntosh and Hendon 2018). They emanate from the tropical Indian Ocean and produce a barotropic pressure center in the SAU, thereby affecting rainfall there through changing the west–east steering, mean-state baroclinicity, and possibly orographic effects (Ashok et al. 2007; Cai et al. 2011). The positive phase of IOD (pIOD) is generally associated with rainfall deficits, and conversely, the negative phase of IOD (nIOD) is associated with wetter-than-normal conditions (Risbey et al. 2009).

However, under the global warming, the emergence of ENSO diversity in the twenty-first century has brought significant changes to ENSO-driven rainfall variability over many areas of Australia (Delage and Power 2020; Cai et al. 2021; Watterson et al. 2021). With the increasing occurrence of events with the SST anomaly (SSTA) peaking in the CP since the late 1990s (Yeh et al. 2009; Lee and McPhaden 2010; Freund et al. 2019), many studies have suggested that a different flavour of El Niño exists, concerning its spatial pattern, thermocline depth, zonal current, intensity, as well as the location of convection (Larkin and Harrison 2005; Ashok et al. 2007; Kao and Yu 2009; Takahashi et al. 2011; Yeh et al. 2014). The El Niño episode with its maximum SSTA concentrated in the CP is referred to as CP El Niño (Kao and Yu 2009). More details about the properties, dynamics, predictability and impacts of ENSO diversity can be seen in reviews of Yeh et al. (2014) and Santoso et al. (2019). Given that large-scale atmosphere teleconnections are sensitive to the critical details of the equatorial SSTA pattern (Barsugli and Sardeshmukh 2002; Capotondi et al. 2015), one might deduce that the influence of an El Niño event depends on its particular flavour (Weng et al. 2007; Alizadeh-Choobari 2017). Specifically, CP ENSO tends to be associated with a more widespread rainfall deficit in Australia than EP- (Ashok et al. 2007; Lim and Hendon 2015; Watterson 2020). Consequently, recent seasonal predictions on Australian rainfall using dynamical models and statistical models focus on predicting both the EP and CP ENSO and their associated influences (O'Kane et al. 2020; Lim et al. 2021b; Watterson et al. 2021). Investigating the cause for the different influences between EP and CP episodes is still an open field of research. But based on the investigation using observations and simulations from dynamical models, the closer forcing center is probably the reason for CP events' more severe influence (Wang and Hendon 2007; Taschetto et al. 2009). For instance, the 1997/98 EP El Niño was near record strength, yet Australian rainfall was near normal. In contrast, the modest 2002/03 CP El Niño event was associated with a severe drought across most parts of Australia (Wang and Hendon 2007). Therefore, investigating the different impacts of both CP and EP El Niño is essential for improving the predictive skill of Australian seasonal rainfall. Also, whether the influence mechanisms of CP and EP

El Niño on Australian rainfall are differential needs further investigation, other than simply analyzing their differences in the induced water vapor conditions as many studies do (e.g., Taschetto et al. 2009). The twenty-first century has witnessed 2 EP El Niño, 2 EP La Niña, 6 CP El Niño and 7 CP La Niña events, revealing that CP ENSO has occurred more frequently during the recent two decades (Lee and McPhaden 2010). Moreover, the warming background climate can result in an increased frequency of ENSO events (Power et al. 2017) as well as an enhancement of ENSO teleconnection and thus its impact (Cai et al. 2015; Power and Delage 2018). Given the higher occurrence frequency of CP El Niño, and its more substantial impact on Australian rainfall compared with EP El Niño in recent two decades, it is important to do further research on CP ENSO-Australian rainfall relationship, which is the core of this article. This article is organized as follows. Section 2 describes the datasets and methods. Section 3 introduces the prolonged drought and reveals the dominant forces of regional rainfall variability on the interannual timescale. Section 4 discusses the specific influence of these dominant forces on Australian spring rainfall. In Sect. 5, analysis is conducted on the mechanisms associated with the distinct influences of CP and EP ENSO on rainfall. The article ends up with summary and discussion in Sect. 6.

2 Data and methodology

2.1 Data description

All datasets in this article range from 1979 to 2020 when more reliable observations are available, except for the SST and Australian rainfall with a period of 1948–2020. We restrict the studied months to austral spring, during which ENSO and IOD are strongly correlated and can have a mutual influence on the Australian climate. ENSO and IOD are monitored by tropical SST variations from the Hadley Centre Global sea ice and SST analyses (HadISST 1.1; Rayner et al. 2003) on an $1° \times 1°$ longitude-latitude grid. The Niño 4, Niño 3.4 and Niño 3 indices are calculated from the average SSTAs of (5°S–5°N, 160°E–150°W), (5°S–5°N, 170°W–120°W), (5°S–5°N, 150°W–90°W), respectively. The IOD is measured by the Dipole Mode Index (DMI), which is the difference between the average SSTAs at IODW(10°S–10°N, 50°E–70°E) and IODE(10°S-Eq, 90°E–110°E).

Geopotential height anomalies at the upper troposphere ascribed to tropical convection variations acting as a Rossby source, are used to diagnose the circulation variations induced by the propagation of barotropic Rossby wave trains. Specific humidity and wind anomalies at the lower troposphere are used to monitor the moisture transport

over the Australian region. The 850 hPa specific humidity, 850 hPa wind and 200 hPa geopotential height (Z200) are provided by the ECMWF Reanalysis version 5 (ERA5; Hersbach et al. 2019) dataset available on the $0.25° \times 0.25°$ grid. We depict the Australian rainfall using the Australian Water Availability Project (AWAP; Jones et al. 2009) dataset provided by the Bureau of Meteorology (BoM). AWAP is a daily reanalysis data with a high spatial resolution of $0.05° \times 0.05°$ based on station observations, which major meteorological organizations have widely used to analyze rainfall. Here we use its monthly total rainfall for analysis. All the time series have been previously detrended over their time periods to avoid the disturbance of long-term trends and focus on their interannual variations. Seasonal anomalies are constructed by subtracting the corresponding climatology of 1981–2010 throughout this article.

2.2 Methodology

Our fundamental analysis techniques involve cluster analysis, composite analysis and correlation analysis. There is a distinctive regional feature in Australian rainfall between that in tropical region and extratropical region, as well as coastal region and inland region. So we employ cluster analysis to partition the Australian rainfall into several clusters based on its interannual variations to find out the distinctive forces of rainfall in each cluster region. Cluster analysis is widely used to group items. Commonly used cluster analysis algorithms are widely categorized into: model-based, grid-based, division-based, centroid-based, hierarchy-based, density-based and subspace-based methods. The K-Means algorithm applied in this article is a centroid-based clustering method (Lloyd 1982) which is the most commonly used grouping algorithm for its simplicity and efficiency. It has been widely implemented in various fields for scientific and industrial applications (Kodinariya and Makwana 2013). K-Means can clearly partition the dataset into K pre-defined non-overlapping subgroups and ensure a high similarity of different objects in the same cluster and a low similarity among different clusters. Its main objective is to minimize the sum of distances (which is defined with squared Euclidean distance here) (Hartigan and Wong 1979).

The way K-Means algorithm works is as follows (Lloyd 1982):

The first step, randomly select K points from the dataset as centroids.

The second step, assign all the points to their closest cluster centroids.

The third step, for each cluster, recompute its centroid by taking the average of all data points that belong to it.

The fourth step involves repeating the second and third steps until there is no change to the centroids and points remain in the same cluster. It needs to be noted that K-Means

is sensitive to the initialization of prototypes and requires a specific clustering number in advance (Naldi et al. 2011). So we apply the K-Means + + algorithm (Arthur and Vassilvitskii 2007) for cluster center initialization, and the elbow method (Nainggolan et al. 2019) to determine the optimal value of K. Elbow method is one of the most popular cluster optimization methods. Its idea is to run K-Means on the data for a series of K values, and for each K value compute the sum of squared error (SSE). As K increases, there will be fewer points in each cluster, and the distances of points and their respective centroids will decrease, SSE will consequently decrease. The value of K at which SSE declines the most is called the elbow, which indicates the optimal cluster number. The SSE formula is as follows:

$$SSE = \sum_{i=1}^{K} \sum_{x_j \epsilon C_i} \|x_j - \mu_i\|^2. \tag{1}$$

Here x_j is the object in the cluster C_i, μ_i is the cluster's centroid, and K is the clustering number. In this study, we first choose the appropriate clustering number with elbow method, then apply K-Means clustering algorithm to the standardized Australian total rainfall and classify the gridded rainfall data into 3 parts, in preparation for the analysis of the key forces of each partition.

Different types of ENSO are quantified by two ENSO indices following the definition of Ren and Jin (2011), with the N_{WP} index measuring the intensity of the CP ENSO and the N_{CT} Index measuring the intensity of the EP ENSO events. The two ENSO indices are introduced here not only because they are able to differentiate the CP and EP types of ENSO (Heidemann et al. 2022), but also because they are basically unrelated so that the Australian rainfall-ENSO relationship of either type will not have the interference of the other one (Ren and Jin 2011). The N_{WP} Index and N_{CT} Index are calculated here utilizing the Niño 3 and Niño 4 indices with a nonlinear transformation:

$$\left\{ \begin{array}{l} N_{WP} = N_4 - \alpha N_3 \\ N_{CT} = N_3 - \alpha N_4 \end{array} \right., \alpha = \left\{ \begin{array}{l} 2/5, N_3 N_4 > 0 \\ 0, otherwise. \end{array} \right. \tag{2}$$

Here, N_3 and N_4 refer to the Niño 3 and Niño 4 indices, respectively. The N_3 and N_4 indices are strongly correlated with a correlation coefficient of 0.76. Thus, in the N_3–N_4 phase space, there is an evident linear relationship between the N_3 and N_4 indices. While after the linear combination of the N_3 and N_4 indices, the correlation between the N_{CT} and N_{WP} index declines to nearly 0. This is because that this transformation methodology is virtually an orthogonal coordinate transformation from the N_3–N_4 into the N_{CT}–N_{WP} phase space. The previous coordinates in the N_3–N_4 space with high values of both N_3 and N_4 will relocate near the horizontal and vertical axes in the new N_{CT}–N_{WP} space after the transformation (Ren and Jin 2011).

ENSO is strongly correlated with the IOD in austral spring, so we employ partial correlation to isolate the respective influence of ENSO and IOD on rainfall, in order to investigate the relative role of ENSO and IOD. In statistics, partial correlations are often used to examine the actual correlation between two factors and eliminate the impact of a third factor. After excluding the impact of factor c, the partial correlation coefficient between factor a and factor b is:

$$R_{ab \cdot c} = \frac{R_{ab} - R_{ac} \cdot R_{bc}}{\sqrt{(1 - R_{ac} \cdot R_{ac})(1 - R_{bc} \cdot R_{bc})}} \quad (3)$$

Here $R_{ab \cdot c}$ is the partial correlation coefficient between a and b, R_{ab}, R_{ac}, R_{bc} is the Pearson Correlation Coefficient between a and b, a and c, b and c, respectively. Based on this equation, we achieve a measure of the actual correlations between rainfall and ENSO indices that are independent of DMI, denoted $N_{WP}|_{DMI}$, Niño $3.4|_{DMI}$ and $N_{CT}|_{DMI}$. Similarly, we define the actual correlations between rainfall and DMI that are uncorrelated to both types of ENSO indices, denoted DMI$|_{Niño\ 3.4}$ (Cai et al. 2011). The direct Pearson Correlation Coefficients between rainfall and these indices are also calculated as comparisons with the partial ones, to show the mutual effect of the ENSO and the IOD on Australian rainfall.

3 Climate drivers of Australian regional rainfall variability

3.1 Brief introduction of the 2017-early 2020 drought

The drought was started southern Queensland and northern New South Wales with moderate intensity in 2017. In 2018 it worsened and propagated to the southeastern quarter of Australian mainland including the southern Queensland, New South Wales, Victoria and eastern South Australia. Then in 2019, Australian rainfall reached its dip at 40% below the average (BoM 2020). New South Wales, SAU, and the MDB have seen the driest year on record (Wittwer 2020). Besides, bushfires burned large areas of Australia with unprecedented intensity and scale from June 2019 to March 2020 (Wittwer and Waschik 2021). From February to April 2020, the rainfall deficits largely reversed through large parts of southeastern Australia and EAU (BoM 2020). As shown in Fig. 1, the most extreme spring rainfall deficiencies during 2018–2019 occurred in the southern inland Queensland and adjacent northern New South Wales located in EAU, leaving people particularly interested in the climate drivers of rainfall in this region, and it will be shown to associate with CP ENSO in the following sections.
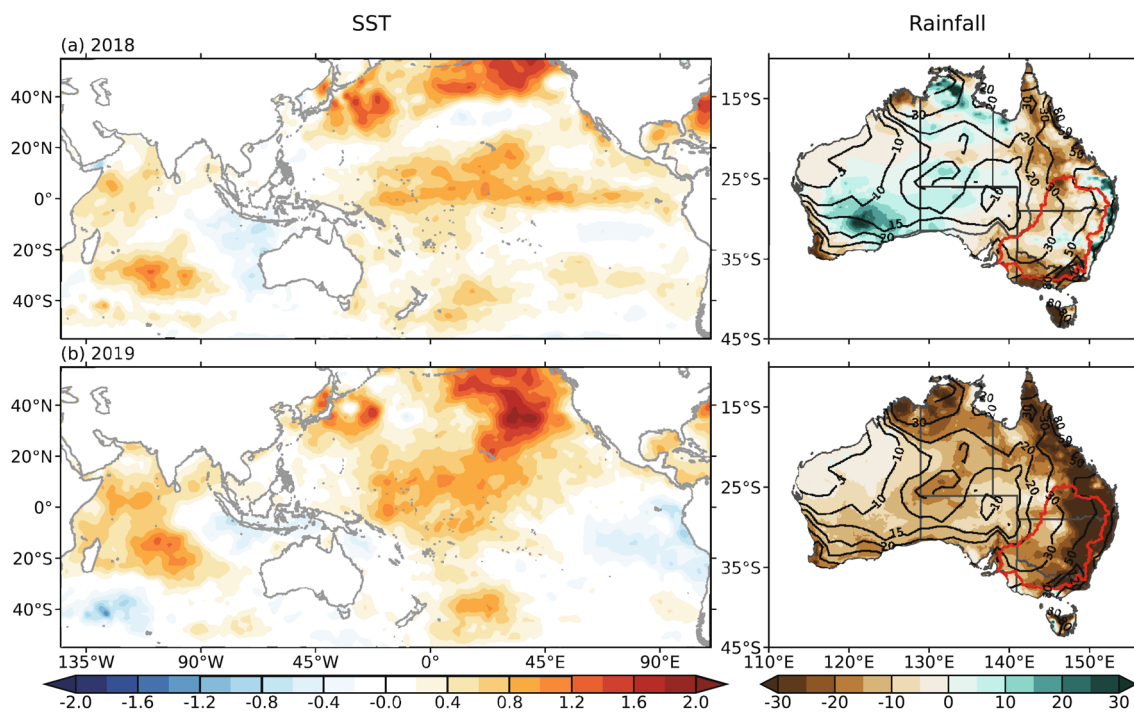

Fig. 1 SSTA and monthly mean total rainfall anomaly (mm/month) for austral spring in **a** 2018 and **b** 2019; the left column is SSTA (shaded) and the right column is Australian rainfall anomaly (shaded). The *black contours* indicate the climatology of monthly mean total rainfall for austral spring. The boundary of the MDB is marked in *red*

3.2 Crucial tropical drivers of the interannual variability of Australian regional rainfall

Since the rainfall deficiencies in austral spring in 2018 and 2019 are known to have close relationship with the long-term rainfall variability, the climate drivers of this rainfall variability are investigated. Considering that the interannual variability of Australian rainfall is regionally specific, we divide the Australian gridded rainfall data into subgroups based on K-Means cluster analysis and investigate its regional characteristics. The determination of clustering number 3 here is defined through elbow method. As shown in Fig. 2b, the elbow is at K = 3, which indicates the optimal clustering number. Based on the interannual variances of rainfall series, the gridpoints are separated into 3 partitions (Fig. 2a), namely western Australia (WAU), SAU and the rest, consisting of NAU, EAU and central inland of Australia. The correlation coefficients between rainfall in these three Cluster regions are further calculated, to examine the coherency and discrepancy of regional rainfall variability across Australia (Table. 1, the first row). The correlation between rainfall in Cluster region 1 and 2 is 0.26, and that between Cluster region 1 and 3 is 0.12. This indicates that rainfall in Cluster region 1 has significantly different interannual variation features with region 2/3. Rainfall in Cluster region 2 and 3 have a significant correlation of 0.67, which means that rainfall variations in these two regions are somewhat consistent. However, if we divide the rainfall time series into two partitions (pre-2000 and post-2000) and employ cluster analysis on them respectively, the correlation between Cluster region 2&3 using pre-2000 data is unsignificant, whereas that of post-2000 data is as high as 0.85 (Table. 1). The pre-2000 and post-2000 cluster analysis results are shown in Fig. S1. Note that the spatial pattern of the pre-2000 period is quite similar to that of the whole

Table 1 Correlation coefficients between Australian area-averaged spring rainfall in three Cluster regions divided by cluster analysis based on AWAP data with three different time periods

	Cluster region 1&2	Cluster region 1&3	Cluster region 2&3
1979–2019	0.26	0.12	**0.67**
Pre-2000	0.27	0.21	0.41
Post-2000	0.21	0.11	**0.85**

The correlation coefficients in bold are significant at the 95% level

period, while that of the post-2000 period manifests a great transformation in the previous Cluster region 2&3. The new Cluster regions 2&3 seem to mix up with each other. This result highlights a transformation on the Australian regional rainfall variability after 2000. Before 2000, rainfall variabilities in Cluster region 2 and 3 are distinct from each other, which means that their drivers and corresponding mechanisms are different. After 2000, they become highly consistent, implying that they might share the same drivers.

Then, we compute the correlation coefficient between rainfall and SST to find out the vital SST areas that can force the interannual variations of rainfall in different regions of Australia. As shown in Fig. 3a, rainfall in WAU (Cluster region 1) is much less affected by SST forcing compared with other regions. It mainly exhibits a moderate negative correlation with SST variations in the off-equatorial central Pacific, with a correlation of −0.48 between rainfall anomalies in WAU and N_{WP} Index (Table 2). Rainfall in NAU, EAU and central inland (Cluster region 2) are substantially forced by the remote SSTs in tropical CP (Fig. 3b). The correlation coefficient spatial pattern of Cluster region 2 resembles the SSTA pattern of CP La Niña, indicating CP ENSO might be a major forcing of interannual rainfall variability in EAU,
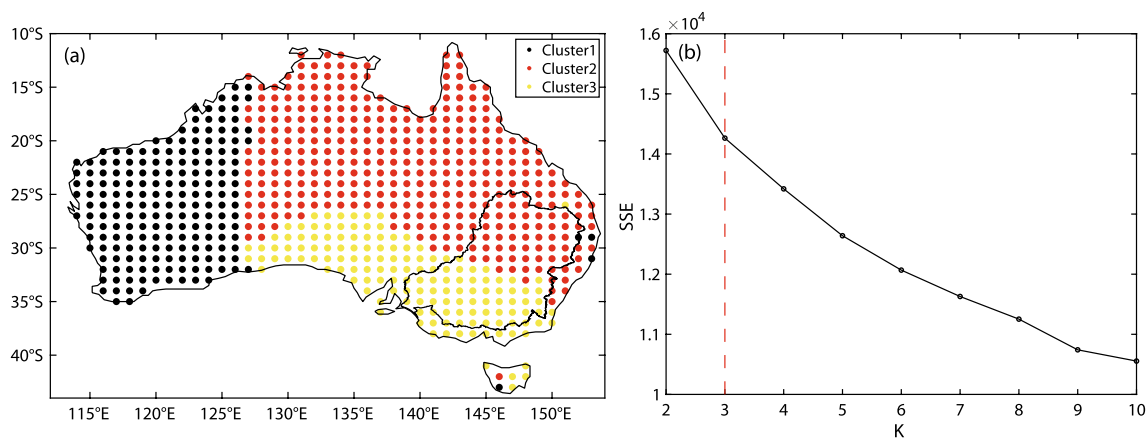

Fig. 2 **a** K-Means cluster analysis on standardized rainfall for austral spring ranging from 1979–2020. The *black*, *red* and *yellow dotted* points are categorized into the first, second and third cluster, respec-

tively. Only $1° \times 1°$ AWAP data is used here. **b** The sum of squared error (SSE) for a range of clustering number K
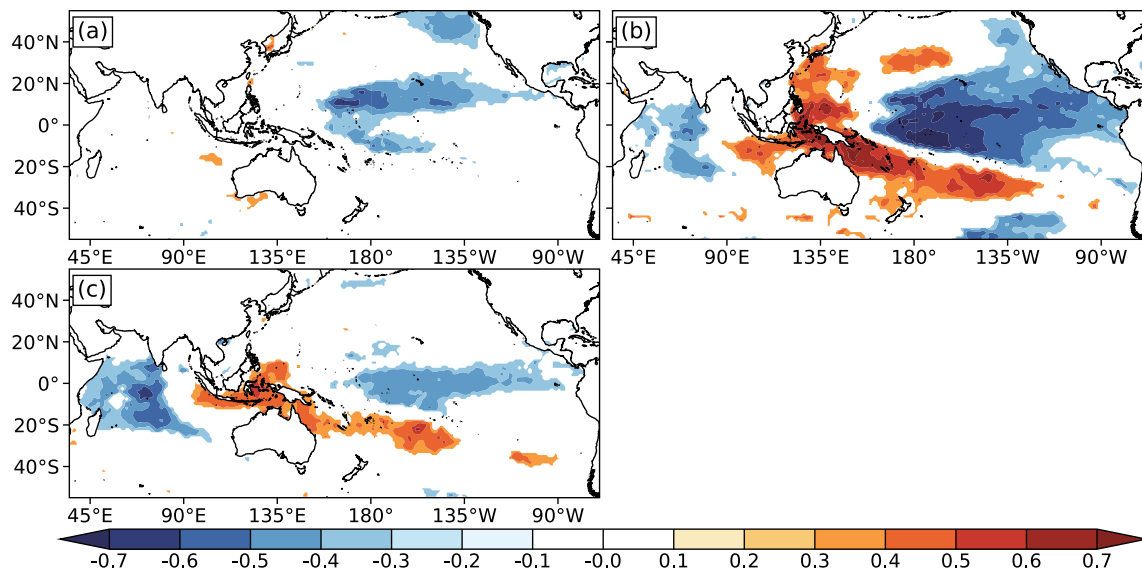
Fig. 3 **a**-**c** are the correlations between SST and averaged rainfall for austral spring in Cluster region 1–3, respectively. The SST and Australian rainfall have been detrended prior to the correlation analysis, with the time periods of 1979–2020. Only correlations significant at the 5% level are shown

Table 2 The correlation coefficients between several indices and area-averaged rainfall anomalies (mm/month) in Cluster region 1–3, all-Australia for austral spring, with the time periods of 1979–2020

	N_{WP} Index	N_{CT} Index	DMI
Cluster region 1	**− 0.48**	− 0.01	− 0.07
Cluster region 2	**− 0.67**	**− 0.45**	**− 0.43**
Cluster region 3	**− 0.39**	**− 0.37**	**− 0.53**
All-Australia	**− 0.68**	**− 0.44**	**− 0.47**

The correlation coefficients in bold are significant at the 95% level

central inland Australia and NAU. Naturally, the correlation between rainfall in this region and the N_{WP} Index is the strongest (-0.67) among all Cluster regions. Rainfall in Cluster region 2 also appears to be moderately correlated with the IOD, though it is considered to be contributed by the strong covariation of the IOD with ENSO in austral spring rather than the independent influence of IOD itself because the effect of the IOD is only confined in extratropical Australia (Cai et al. 2011). Rainfall in SAU (Cluster region 3) has a noticeable relationship with SSTs in the two dipoles of IOD (Fig. 3c), revealing that a positive phase of the IOD (pIOD) would bring rainfall deficiencies to SAU, and vice versa for a negative phase of the IOD (nIOD), confirming the result of Cai et al. (2011). There is no doubt that the correlation between rainfall anomalies in SAU and IOD is the strongest (-0.53) among all Cluster regions. Rainfall in Cluster region 3 is also shown to moderately feel the impact from SST variations in equatorial CP (Fig. 3c), which might stem

from the strong coherence between ENSO and IOD during austral spring (Cai et al. 2011). Furthermore, local SSTs off the coast of NAU also have a considerable coherence with rainfall in NAU, EAU and SAU, though some suggested that the north Australian SSTs act as an agent for conveying the impact of variability coherent with CP ENSO (van Rensch and Cai 2014). It should be noticed that, the CP ENSO has a more severe impact on Australian rainfall in all three regions of Australia as well as the whole Australia than EP- (Table. 2). This is particularly evident in WAU, with correlation of WAU rainfall-N_{WP} Index being significant while that of western Australian rainfall-N_{CT} Index close to zero. In general, Australian spring rainfall is highly consistent with the tropical Indo-Pacific SSTs across most regions of Australia, with rainfall in WAU, NAU and EAU closely correlated with CP ENSO and rainfall in SAU more correlated with the IOD.

These correlation results imply that the 2018–2019 rainfall decline is probably attributed to CP El Niño and pIOD if they occurred. Here we define a pIOD event using + 0.7 times the standard deviation (s.d.) of DMI in austral spring as the threshold to achieve more event samples for composite analysis following the definitions of many research (e.g., Yuan and Yamagata 2015). According to Ren and Jin (2011) and Heidemann et al. (2022), the years in which N_{WP} index/ N_{CT} index for austral spring greater than + 1 s.d. are regarded here as years of the CP El Niño/EP El Niño. According to this definition, the years of pure pIOD, CP El Niño&pIOD, EP El Niño&pIOD ranging from 1948–2020 are shown in Table 3, with the values of associated indices for austral spring listed in the brackets. Notably, 2018 and 2019 are

Table 3 Pure pIOD years, CP El Niño&pIOD and EP El Niño&pIOD co-occurring years defined by N_{WP} / N_{CT} Index and DMI of austral spring; the values in the brackets indicate the DMI for pure pIOD, N_{WP} Index & DMI for CP-El Niño&pIOD, and N_{CT} Index & DMI for EP-El Niño&pIOD in austral spring

Pure pIOD	CP-El Niño & pIOD	EP-El Niño & pIOD
1961 (0.77)	1987 (0.45 & 0.38)	1951 (1.08 & 0.36)
1963 (0.59)	1994 (0.59 & 0.65)	1972 (1.79 & 0.71)
1967 (0.40)	2002 (0.42 & 0.36)	1982 (2.09 & 0.65)
2006 (0.57)	2018 (0.40 & 0.60)	1987 (1.00 & 0.38)
2011 (0.34)	2019 (0.58 & 0.90)	1997 (2.70 & 1.10)
		2015 (1.89&0.40)

both CP El Niño&pIOD years. The SSTA spatial distribution for austral spring in 2018 and 2019 is shown in the left column of Fig. 1, exhibiting a typical pIOD-SSTA pattern over the tropical Indian Ocean in both two years. In particular, from 2018 to 2019, both of the CP ENSO and IOD have substantially increase in their magnitudes (Table 3), together contributing to a more severe drought across the whole Australia in SON 2019 (Fig. 1b; Table 4). Therein, the 2019 pIOD event is amongst the most severe IOD events on record (Wang et al. 2020), with a DMI anomaly of +0.90 °C for austral spring, more than two times the s.d. (0.38 °C). The 2018 pIOD was not that extreme, but still fairly strong, with the DMI at +0.60 °C for austral spring. And SAU experienced severe rainfall deficiencies in austral spring in both 2018 and 2019. In austral spring of both years, there is also a CP El Niño-SSTA pattern in the CP (Fig. 1b) (Wang and Cai 2020; BoM 2020), despite its weak strength in 2018 with a magnitude of +0.40 °C (Table 3). Rainfall in EAU, central inland Australia and NAU significantly decreased in austral spring of both years (Table 4), underlining a possible connection of CP ENSO to rainfall anomalies in these regions.

4 The influences of CP ENSO and IOD on Australian spring rainfall

The previous section has shown that austral spring rainfall in SAU is significantly associated with the IOD, and rainfall in NAU, EAU and central inland of Australia is significantly associated with CP ENSO. To further understand the

footprints of CP ENSO and IOD, we first examine the correlation patterns of rainfall anomalies associated with DMI, ENSO indices, and partial correlation patterns based on Eq. (3) (shown in Fig. 4). Note that the correlation between N_{WP} and N_{CT} index is only about 0.18, so the relationship of either CP or EP El Niño with Australian rainfall can be seen as being independent of the other one. Since the correlations of DMI and ENSO indices do not exclude the influence of each other, their correlation coefficients consist of their covariant part. In contrast, the partial correlation coefficients
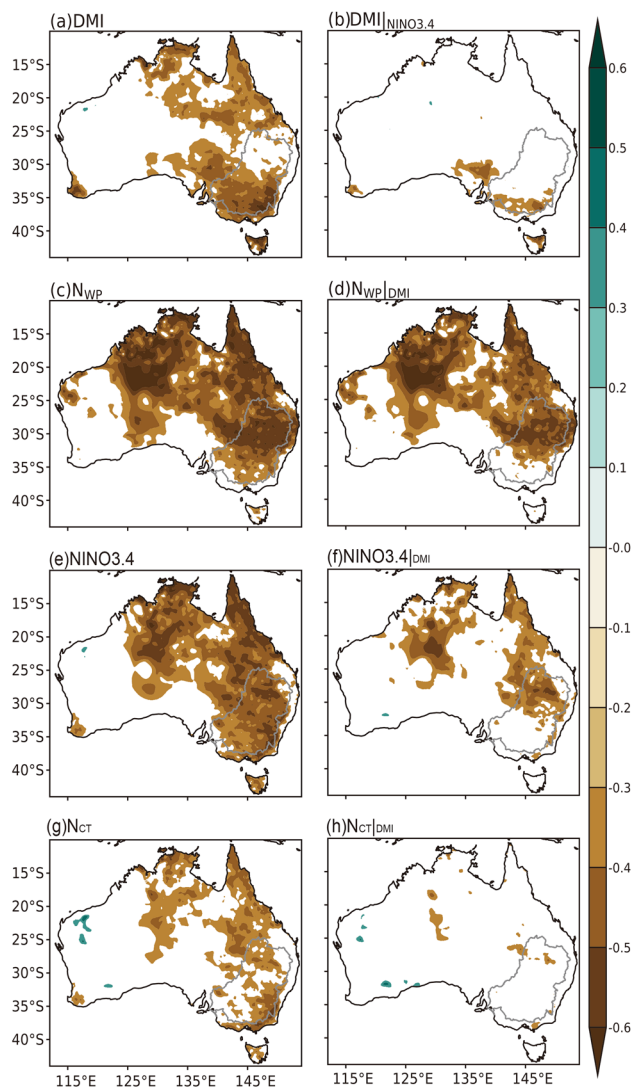

Fig. 4 Correlation coefficients between DMI, N_{WP} Index, Niño 3.4, N_{CT} Index and total rainfall (mm/month) for austral spring are shown in panels **a**, **c**, **e**, **g**, respectively; partial correlation coefficients are shown in panels **b**, **d**, **f**, **h**. Only correlations statistically significant at the 95% confident interval are plotted here. DMI$_{NINO3.4}$ denotes the partial correlation coefficient between DMI and Australian rainfall independent of Niño 3.4; $N_{WP}|_{DMI}$, NINO3.4$|_{DMI}$ and N_{CT} |$_{DMI}$ denote the partial correlation coefficient between N_{WP} Index, Niño 3.4, N_{CT} Index and Australian rainfall independent of DMI, respectively

Table 4 Area-averaged rainfall anomalies (mm/month) of Cluster region 1–3 and All-Australia for 2018 and 2019 in austral spring

Year	Cluster region 1	Cluster region 2	Cluster region 3	All-Australia
2018	0.29	− 5.00	− 5.70	− 3.69
2019	− 11.22	− 21.35	− 16.17	− 17.50

reflect the independent correlations of the IOD or ENSO with precipitation. When calculating the partial correlation coefficient between DMI and rainfall, the Niño 3.4 index's impact is removed from the DMI-rainfall correlation as a representation of the intermediate state of CP and EP ENSO.

As presented in the correlation/partial correlation results, there is a significant CP ENSO-rainfall teleconnection across most of Australia (Fig. 4d), yet the teleconnection of EP ENSO is much weaker and appears to be insignificant in large areas of Australia (Fig. 4h). The cooperation with the IOD can largely enhances the influence of EP ENSO (Fig. 4g), but only has subtle effect in extending the influence of CP ENSO towards far south. There are broad rainfall responses, including tropical and extratropical ones, to N_{WP} Index across EAU, NAU and central inland of Australia (Fig. 4d). Nevertheless, the response to N_{CT} Index is quite limited to NAU (Fig. 4g), indicating that only tropical effects associated with EP ENSO exist, although far less than CP. In particular, rainfall shows correlation of up to -0.5 with N_{WP} Index in EAU (Fig. 4d), indicating that variations of rainfall in this region are dominated by CP ENSO. Generally speaking, no matter whether an IOD event is coexisting with ENSO event or not, the closer the forcing center in the equatorial Pacific is to Australia, the stronger its effect is on spring rainfall over Australia (Fig. 4c–h). Both the

tropical and extratropical effects of CP ENSO are much stronger than EP's.

Unlike ENSO whose impact is distributed in lower latitude of Australia, the IOD mainly impacts rainfall in higher latitude. Both ENSO and IOD have little impact on most of WA except for the southwest corner (Fig. 4). The IOD and ENSO tend to increase each other's impact intensity and extent in austral spring. With the participation of ENSO, IOD can extend its influence scope towards lower latitude. So does ENSO, with IOD's assistance, the scope of its influence extends towards higher latitude, in agreement with the results of Watterson (2020). Together with pIOD, CP El Niño is able to bring severe and broad rainfall deficiencies in EAU, SAU and NAU, which is mostly the condition of the Australian spring drought in 2018 and 2019.

To have a clearer picture of the difference between CP and EP's imprints, we then carry out the composite analysis to the CP and EP El Niño episodes based on the event years in Table 3. Only the composites of the positive phase are conducted here because the coherence between nIOD and La Niña is much lower than that of the positive phase (Cai et al. 2012), such that the cases are too few to be compounded. The composite SSTA patterns for CP/EP El Niño and pIOD are shown in Fig. 5, with the maximum warming center situated in the central and eastern equatorial Pacific, respectively. And the corresponding rainfall patterns of the
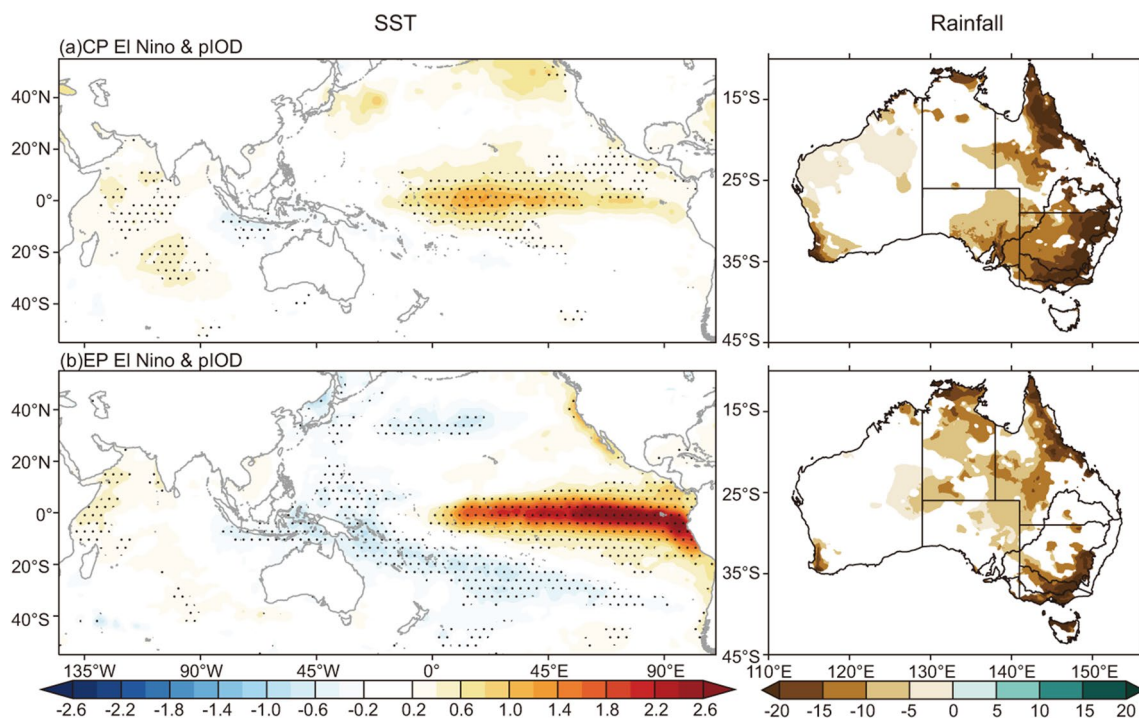

Fig. 5 Composites of SST and total rainfall anomalies (mm/month) for austral spring in **a** CP El Niño&pIOD co-occurring years, **b** EP El Niño&pIOD co-occurring years. *Dotted areas* indicate significant composite at the 95% confident interval. *Shaded region* in the right column has significant composite anomalies at the 95% confidence level

two types show a noteworthy difference in the subtropical EAU, where the CP El Niño is associated with significant deficiencies while EP El Niño lacks an extratropical rainfall response. These composite results are coherent with the rainfall-N_{WP} Index and rainfall-N_{CT} Index correlations above, confirming that the impact of the CP El Niño is distinct from the EP's, especially in EAU.

5 Discrepancy on the CP&EP ENSO's influence mechanisms on extratropical Australian rainfall

Last section has shown that Australian regional rainfall responses differently to CP and EP ENSO. To be specific, CP ENSO has a broader and stronger impact on Australian spring rainfall than EP ENSO with or without the aid of the IOD, and rainfall in EAU can only be affected by the CP type. Next, we will show the possible mechanisms underlying the influences of the two types.

The correlation patterns of 200 hPa geopotential height associated with the N_{WP} Index, Niño 3.4, N_{CT} Index, DMI and $N_{WP}|_{DMI}$, Niño 3.4$|_{DMI}$, $N_{CT}|_{DMI}$, DMI$|_{Niño\ 3.4}$ for austral spring are shown in Fig. 6. The anomalous high pressure center near SAU is pronounced during IOD in Fig. 6a, b, extending from the upper layer to the lower layer (Fig. 6–7a). This anomalous pressure center still exists under the IOD and EP ENSO co-occurring situation (Fig. 6g), and is absent after removing the covariant part of IOD and ENSO from the ENSO-rainfall correlation (Fig. 6d, f, h). It is also significant on the surface layer during IOD (Fig. S2a, b), and manifests as a stretch of the SO west branch towards higher latitude of Australia when IOD and EP ENSO co-occur (comparing Fig. S2e, g with Fig. S2f, h). This barotropic anomalous height center, induced by equivalent-barotropic Rossby wave trains emanating from the tropical eastern Indian Ocean, accounts for the rainfall anomaly in SAU during IOD events
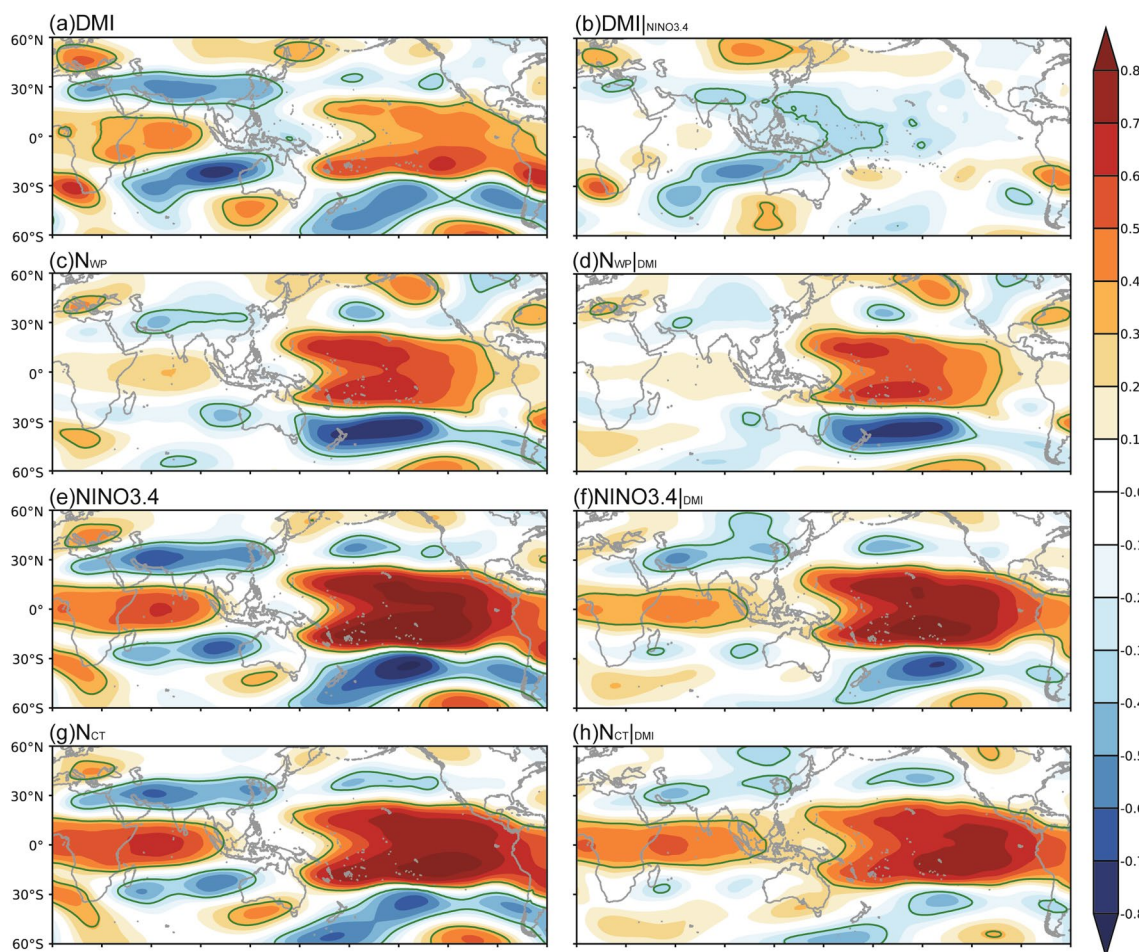

Fig. 6 Correlation coefficients between DMI, N_{WP} Index, Niño 3.4, N_{CT} Index and 200 hPa geopotential height for austral spring are shown in panels **a**, **c**, **e**, **g**, respectively; partial correlation coefficients are shown in panels **b**, **d**, **f**, **h**. Green real contours encompass the statistically significant correlations at the 95% confident interval
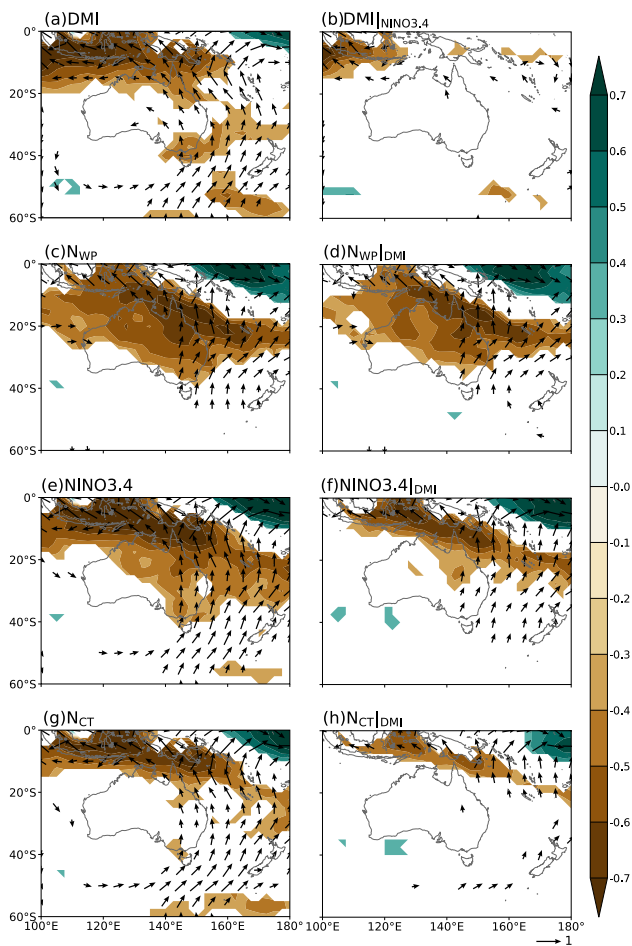
Fig. 7 Correlation coefficients between DMI, N_{WP} Index, Niño 3.4, N_{CT} Index and the specific humidity (kg/kg), wind (m/s) on 850 hPa for austral spring are shown in panels **a**, **c**, **e**, **g**, respectively; partial correlation coefficients are shown in panels **b**, **d**, **f**, **h**. The *black vectors* show significant values in at least one wind component at the 95% confidence level. *Shaded regions* have correlations significant at the 95% confidence interval

(Fig. 4a, b, e, g), consistent with Cai et al. (2011). It is worth noticing that, during CP ENSO the anomalous height center over SAU is absent, even when CP ENSO is co-occurring with IOD (Fig. 6c). This implies that during a CP event, the Indian Ocean no longer plays a significant role in conveying the impact of CP ENSO to SA as it does in an EP event. The mechanism of ENSO-IOD-Southern Australian rainfall teleconnection put forward by Cai et al. (2011) is virtually only applied to the EP ENSO case. The impact of CP ENSO on extratropical Australia does not stem from the barotropic Rossby wave train emanating from the Indian Ocean, but rather from the remote impact from equatorial CP.

The distribution of 200 hPa geopotential height in the Southern Pacific features a tropical high-pressure center and a subtropical low-pressure center stretching across the Pacific Ocean basin (Fig. 6), constituting part of the so-called Pacific-South American (PSA; Hoskins and Karoly 1981) pattern. The PSA pattern is induced by the propagation of equivalent barotropic waves emanating from upper-level divergence over the equatorial CP. As presented in Fig. 6c, d, g, h, although the PSA pattern appears to be notable for El Niño of both types, the one associated with the CP El Niño possesses a more zonal structure and is more westward compared to EP-. The CP El Niño-related negative 200 hPa geopotential height anomalies in the subtropical Pacific stretches to the eastern coast of the Australia continent. Given that the anomalous height center over SA related to the IOD is absent during CP ENSO no matter co-occurring with IOD or not (Fig. 6c, d), the extratropical impact of CP ENSO on eastern Australian rainfall (Fig. 4c, d) can only be conducted through the subtropical PSA. As for EP ENSO, the Rossby wave train response is trapped in the Pacific (Fig. 6g, h), and thus little rainfall response is felt in EAU (Figs. 4h, 5b). This explains why EA lacks a rainfall signal during EP El Niño&pIOD events (Fig. 5). Moreover, the PSA pattern that we focus on also tends to be stronger during CP El Niño because of the interaction of background and disturbance field. Specifically, the convective center of CP El Niño is situated closer to the ascending branch of Walker Circulation so that it is easier for the perturbation to be transported to the upper-level atmosphere and propagate out as a wave train. In contrast, the convective center of EP El Niño is situated closer to the descending branch, where it is difficult for the perturbation to be brought to the upper atmosphere and neither for the following propagation. Consequently, the equivalent wave trains are able to convey the impact of CP El Niño to rainfall in EAU and significantly contribute to the rainfall variability there, which is yet unavailable for EP El Niño.

With regard to NAU, it is covered by anomalous high pressure associated with the western pole of SO on the surface for both two types of ENSO (Fig. S2c, d, g, h), indicating that El Niño influences rainfall in NAU through weakening the ascending branch of Walker Cell located around the Maritime Continent. What's more, the adverse wind direction in the upper level and lower level above equatorial northeastern Australia and western Pacific during ENSO reveals that the atmosphere here is baroclinic. As such, rainfall in equatorial NAU is affected by El Niño of both types via SO rather than PSA pattern.

The responses of lower-level atmosphere to CP and EP ENSO above Australia seem to be more distinct than the upper level. Figure 7 depicts the correlations between 850 hPa wind and specific humidity with the indices. As the results exhibit, the CP type has a higher correlation with atmospheric circulation anomalies than EP- (Figs. 6-7c, d, g, h), as the atmosphere tends to be more sensitive to SSTAs in CP with warmer surface and more active atmospheric convection activities and less responsive to SSTAs in EP

situated in the cold tongue (Barsugli and Sardeshmukh 2002). Therefore, the rainfall-CP El Niño coherence is substantially higher than the EP type (Fig. 4c, d, g, h), no matter in the tropical or extratropical Australia. During CP El Niño, rainfall in EAU is dominated by significant southerly offshore lower-level flow whether co-occurring with the pIOD or not (Fig. 7c, d), which carries less moisture from the dry cold higher-latitude region to lower-latitude region, and results in a dryer-than-normal condition in EAU (Fig. 4c, d), in agreement with Watterson (2020).

Moreover, the southerly wind in EAU is considered to be induced by the barotropic Rossby wave train emanating from CP, because EAU and part of SAU is exactly located under the western margin of the low pressure associated with the extratropical PSA pattern (Fig. 6c, d). But for EP El Niño, there is basically little significant southerly wind and moisture anomalies in EAU (Fig. 7h), associated with little rainfall signal in this region (Fig. 4h). To the east of New Guinea, the lower-level wind represents a cyclonic circulation pattern, while the upper-level wind pattern appears to be anticyclonic (figure not shown). The contrast of lower-level atmospheric circulation between the two types of ENSO is ultimately attributed to their different SSTA patterns in the Pacific. Since the SSTA center of CP El Niño is closer to Australia, the associated anomalous convective heating center is closer, and the emanated barotropic Rossby wave train response associated with the PSA pattern are closer too. Thus, the wave train of CP type is able to affect the general atmospheric circulation above EAU when propagating into the extratropical Southern Hemisphere. It sparks anomalies of negative higher-level geopotential height as well as southerly lower-level wind associated with the subtropical PSA pattern over EAU, thereby reducing the water availability and consequently the austral spring rainfall in this area. In comparison, the extratropical PSA pattern of EP ENSO is located too far east to affect the EAU, such that EP ENSO can only exert influence on SAU with IOD's assistance (Cai et al. 2011). Finally, it appears that the rainfall anomaly patterns of CP and EP ENSO in EAU are distinct (Fig. 4c, d, g, h and the right column of Fig. 5).

When El Niño and IOD coexist, the southerly flow along the western edge of the extratropical PSA pattern associated with ENSO would also contribute to the rainfall deficits in southeastern Australia (left column of Fig. 7). Although Cai et al. (2011) had suggested that the rainfall variances in SAU are caused by IOD-induced high-pressure center that obstructs the rain-bearing eastward-moving weather systems moving towards SAU, here the emphasis is made on the role of ENSO on Australian spring rainfall. As shown in Fig. 7(a, b), in the absence of ENSO, IOD has little significant correlation with the 850 hPa wind. But in the presence of both ENSO and IOD, there is not only an IOD-induced high-pressure center but also remarkable southerly wind over

SAU contributed by the extratropical PSA pattern associated with ENSO, weakening the transport of moisture to SAU, consistant with Freund et al. (2021).

6 Conclusions and discussions

6.1 Conclusions

To understand the serious 2018–2019 drought in austral spring on the interannual timescale, this article identifies the SST sources (ENSO and IOD) of interannual Australian regional rainfall variability for austral spring. Cluster analysis result has shown that rainfall variations in different regions are driven by distinctive SST modes. Specifically, spring rainfall variability in Cluster region 1 (WAU) and Cluster region 2 (northeastern half of Australia) is most closely related to CP ENSO, and that in Cluster region 3 (SAU) is most strongly coherent with the IOD. Then, the impacts of CP/EP ENSO and IOD on Australian spring rainfall are discussed, with an emphasis on contrasting the footprints of CP and EP ENSO. We have argued that the ENSO-rainfall teleconnection of CP and EP type has distinctive spatial patterns in Australia, especially in EAU. Specifically, CP El Niño is associated with rainfall deficits across the northeastern half of Australia, while the signal of EP El Niño is much weaker, almost insignificant at a 95% confident level after removing its covariant part with IOD. Since 2000, the rainfall variability in many areas of Australia has changed, which is proven by the substantially higher coherence of rainfall variances in Cluster region 2 and 3 based on cluster analysis using data after 2000. This could be due to the occurrence of an abundance of CP El Niño episodes in recent decades (Lee and McPhaden 2010), which induce a shift on the ENSO-related part of rainfall variability in Cluster region 2.

A critical contribution of the present work is an enhanced understanding of the mechanism by which CP ENSO significantly affects eastern Australian rainfall in contrast to EP-. Our findings indicate that, since the SSTA patterns differ between the two cases, the resulting atmospheric circulation anomalies and their climate effects have distinctive spatial distributions (Ashok et al. 2007; Weng et al. 2007). Generally, the response of Australian rainfall to CP ENSO is greater compared with EP ENSO because the atmosphere is more sensitive to the SSTA closer to the warm pool, confirming the results of Santoso et al. (2019). Compared to EP ENSO, the CP event is consistent with a more significant and closer situated ENSO-induced PSA pattern to Australia. The western edge of the PSA pattern during CP ENSO is associated with lower-level southerly flow bringing dry cold air from the higher latitude and induces rainfall deficiencies in EAU, resulting in a significant CP ENSO-Australian rainfall

teleconnection in this area. In contrast, during EP ENSO, little rainfall variance is presented in EAU, associated with insignificant 850 hPa wind anomalies. This might be attributed to its corresponding PSA pattern which is weaker and sits far too east in the Pacific to convey the variability of EP ENSO to extratropical Australia. Apart from that, our results indicate that the ENSO-southern Australian spring rainfall teleconnection mechanism in Cai et al. (2011) can only be applied to EP ENSO. During CP ENSO, the role of tropical Indian Ocean as an agency to convey the impact from ENSO to southern Australia vanishes. This is demonstrated by the disappearance of the anomalous height center over SAU when CP ENSO is co-occurring with IOD (Fig. 6c). In general, CP ENSO can influence extratropical Australia directly through the PSA pattern, whereas EP ENSO need an IOD to convey its impact to SAU.

6.2 Discussions

This study has an important implication that, a detailed simulation and predictive skill of ENSO diversity from coupled general circulation models (GCM) is critical for advancing the predictive capability of Australian seasonal rainfall. Since CP and EP ENSO have distinctive impact patterns on Australian spring rainfall, only models that have a good predictive skill of both CP and EP ENSO can make accurate forecast on Australian seasonal rainfall. Also, as CP ENSO manifests itself as a more important driver for Australian rainfall variability relative to EP-, it seems to be a more critical source of Australian rainfall predictability. With more CP events occurring in recent decades (Capotondi et al. 2015), the EAU, which was mostly kept from the influence of traditional EP ENSO, now are more likely to suffer from widespread and severe droughts or floods during CP ENSO in austral spring. Most of Australia, including NAU, the central inland and EAU, tend to feel a greater impact from ENSO. As the warming background is conductive to ENSO teleconnection and consequently its impact (e.g., Santoso et al. 2019), the NAU also becomes more exposed to extreme weather associated with CP ENSO. Therefore, predicting the explicit flavour of ENSO events is beneficial to influence preparedness over Australia (Dong and Dong 2021).

This study is based on the assumption that the ENSO and IOD as well as their effects are linear and ignore their asymmetry. Actually, there is not only a significant skewness in ENSO and IOD themselves, but also in their relationships with Australian spring rainfall (Power et al. 2006; Cai et al. 2012; King et al. 2013; Chung and Power 2017), which warrants further investigations. Additionally, this work only focuses on the role of ENSO and IOD, while other modes can also force the interannual variability of Australian rainfall, such as the SAM (Watterson 2020; Lim et al. 2021a), subtropical ridge (Timbal and Drosdowsky 2013) and the

SSTs around NAU which can exert influence on Australian rainfall through the coherence with ENSO (van Rensch and Cai 2014). These are additional issues needing further research in our future work.

Declarations

References

Alizadeh-Choobari O (2017) Contrasting global teleconnection features of the eastern Pacific and central Pacific El Niño events. Dyn Atmos Oceans 80:139–154

Arthur D, Vassilvitskii S (2007) K-means++: the advantages of careful seeding In: Proceedings of the Eighteenth Annual ACM-SIAM Symposium on Discrete Algorithms. SODA'07, Society for Industrial and Applied Mathematics, 1027–1035, Philadelphia, PA, USA

Ashok K, Guan Z, Yamagata T (2003) Influence of the Indian Ocean Dipole on the Australian winter rainfall. Geophys Res Lett 30(15). https://doi.org/10.1029/2003GL017926

Ashok K, Behera SK, Rao SA, Weng H, Yamagata T (2007) El Niño Modoki and its possible teleconnection. J Geophys Res Oceans 112(C11). https://doi.org/10.1029/2006JC003798

Australian Government Bureau of Meteorology (BoM) (2020) Special Climate Statement 70—drought conditions in Australia and impact on water resources in the Murray–Darling Basin. Bureau of Meteorology. http://www.bom.gov.au/climate/current/statements/. Accessed 13 Aug 2020

Barsugli JJ, Sardeshmukh PD (2002) Global atmospheric sensitivity to tropical SST anomalies throughout the Indo-Pacific basin. J Clim 15:3427–3442

Cai W, van Rensch P, Cowan T, Hendon HH (2011) Teleconnection pathways of ENSO and the IOD and the mechanisms for impacts on Australian rainfall. J Clim 24:3910–3923

Cai W, van Rensch P, Cowan T, Hendon HH (2012) An asymmetry in the IOD and ENSO teleconnection pathway and its impact on Australian climate. J Clim 25:6318–6329

Cai W, Santoso A, Wang G, Yeh S-W, An S-I, Cobb KM, Collins M, Guilyardi E, Jin F-F, Kug J-S (2015) ENSO and greenhouse warming. Nat Clim Chang 5:849–859

Cai W, Santoso A, Collins M, Dewitte B, Karamperidou C, Kug J-S, Lengaigne M, McPhaden MJ, Stuecker MF, Taschetto AS (2021) Changing El Niño-Southern Oscillation in a warming climate. Nat Rev Earth Environ 2:628–644

Capotondi A, Wittenberg AT, Newman M, Di Lorenzo E, Yu J-Y, Braconnot P, Cole J, Dewitte B, Giese B, Guilyardi E (2015) Understanding ENSO diversity. Bull Am Meteorol Soc 96:921–938

Chung CT, Power SB (2017) The non-linear impact of El Niño, La Niña and the Southern Oscillation on seasonal and regional Australian precipitation. J South Hemisphere Earth Syst Sci 67:25–45

Delage FP, Power SB (2020) The impact of global warming and the El Niño-Southern Oscillation on seasonal precipitation extremes in Australia. Clim Dyn 54:4367–4377

Dong T, Dong W (2021) Evaluation of extreme precipitation over Asia in CMIP6 models. Clim Dyn 57:1751–1769

Freund MB, Henley BJ, Karoly DJ, McGregor HV, Abram NJ, Dommenget D (2019) Higher frequency of Central Pacific El Niño events in recent decades relative to past centuries. Nat Geosci 12:450–455

Freund MB, Marshall AG, Wheeler MC, Brown JN (2021) Central Pacific El Niño as a precursor to summer drought-breaking rainfall over southeastern Australia. Geophys Res Lett 48:e2020GL091131

Hartigan JA, Wong MA (1979) Algorithm AS 136: a k-means clustering algorithm. J R Stat Soc: Ser C (Appl Stat) 28:100–108

Heidemann H, Ribbe J, Cowan T, Henley BJ, Pudmenzky C, Stone R, Cobon DH (2022) The influence of interannual and decadal Indo-Pacific sea surface temperature variability on Australian monsoon rainfall. J Clim 35:425–444

Hersbach H, Bell B, Berrisford P, Biavati G, Horányi A, Muñoz Sabater J, Nicolas J, Peubey C, Radu R, Rozum I, Schepers D, Simmons A, Soci C, Dee D, Thépaut JN (2019) ERA5 monthly averaged data on pressure levels from 1979 to present, Copernicus Climate Change Service (C3S) Climate Data Store (CDS). https://doi.org/10.24381/cds.f17050d7

Hoskins BJ, Karoly DJ (1981) The steady linear response of a spherical atmosphere to thermal and orographic forcing. J Atmosph Sci 38:1179–1196

IPCC (2021) Weather and Climate Extreme Events in a Changing Climate. In Climate Change 2021: The Physical Science Basis. Contribution of Working Group I to the Sixth Assessment Report of the Intergovernmental Panel on Climate Change. Cambridge University Press, Cambridge, pp 1662–1666. https://www.ipcc.ch/report/sixth-assessment-report-working-group-i/. Accessed 9 Aug 2021

Jones DA, Wang W, Fawcett R (2009) High-quality spatial climate data-sets for Australia. Aust Meteorol Oceanogr J 58:233

Kao H-Y, Yu J-Y (2009) Contrasting eastern-Pacific and central-Pacific types of ENSO. J Clim 22:615–632

King AD, Alexander LV, Donat MG (2013) Asymmetry in the response of eastern Australia extreme rainfall to low-frequency Pacific variability. Geophys Res Lett 40:2271–2277

King AD, Klingaman NP, Alexander LV, Donat MG, Jourdain NC, Maher P (2014) Extreme rainfall variability in Australia: patterns, drivers, and predictability. J Clim 27:6035–6050

King AD, Donat MG, Alexander LV, Karoly DJ (2015) The ENSO-Australian rainfall teleconnection in reanalysis and CMIP5. Clim Dyn 44:2623–2635

King AD, Hudson D, Lim EP, Marshall AG, Hendon HH, Lane TP, Alves O (2020) Sub-seasonal to seasonal prediction of rainfall extremes in Australia. Q J R Meteorol Soc 146:2228–2249

Kodinariya TM, Makwana PR (2013) Review on determining number of Cluster in K-Means Clustering. Int J 1:90–95

Larkin NK, Harrison D (2005) On the definition of El Niño and associated seasonal average US weather anomalies. Geophys Res Lett 32(13). https://doi.org/10.1029/2005GL022738

Lee T, McPhaden MJ (2010) Increasing intensity of El Niño in the central-equatorial Pacific. Geophys Res Lett 37(14). https://doi.org/10.1029/2010GL044007

Lim E-P, Hendon HH (2015) Understanding the contrast of Australian springtime rainfall of 1997 and 2002 in the frame of two flavors of El Niño. J Clim 28:2804–2822

Lim E-P, Hendon HH, Zhao M, Yin Y (2017) Inter-decadal variations in the linkages between ENSO, the IOD and south-eastern Australian springtime rainfall in the past 30 years. Clim Dyn 49:97–112

Lim E-P, Hendon HH, Butler AH, Thompson DW, Lawrence ZD, Scaife AA, Shepherd TG, Polichtchouk I, Nakamura H, Kobayashi C (2021a) The 2019 Southern Hemisphere stratospheric polar vortex weakening and its impacts. Bull Am Meteorol Soc 102:E1150–E1171

Lim E-P, Hudson D, Wheeler MC, Marshall AG, King A, Zhu H, Hendon HH, de Burgh-Day C, Trewin B, Griffiths M (2021b) Why Australia was not wet during spring 2020 despite La Niña. Sci Rep 11:1–15

Lloyd S (1982) Least squares quantization in PCM. IEEE Trans Inf Theory 28:129–137

McIntosh PC, Hendon HH (2018) Understanding Rossby wave trains forced by the Indian Ocean Dipole. Clim Dyn 50:2783–2798

Nainggolan R, Perangin-angin R, Simarmata E, Tarigan AF (2019) Improved the performance of the K-means cluster using the sum of squared error (SSE) optimized by using the Elbow method. In: Journal of Physics: Conference Series, vol 1. IOP Publishing

Naldi MC, Campello RJ, Hruschka ER, Carvalho A (2011) Efficiency issues of evolutionary k-means. Appl Soft Comput 11:1938–1952

Nicholls N (1985) Impact of the Southern Oscillation on Australian crops. J Climatol 5:553–560

O'Kane TJ, Squire DT, Sandery PA, Kitsios V, Matear RJ, Moore TS, Risbey JS, Watterson IG (2020) Enhanced ENSO prediction via augmentation of multimodel ensembles with initial thermocline perturbations. J Clim 33:2281–2293

Power SB, Delage FP (2018) El Niño-Southern Oscillation and associated climatic conditions around the world during the latter half of the twenty-first century. J Clim 31:6189–6207

Power S, Haylock M, Colman R, Wang X (2006) The predictability of interdecadal changes in ENSO activity and ENSO teleconnections. J Clim 19:4755–4771

Power SB, Delage FP, Chung CT, Ye H, Murphy BF (2017) Humans have already increased the risk of major disruptions to Pacific rainfall. Nat Commun 8:1–7

Ramsay H, Richman M, Leslie L (2017) The modulating influence of Indian Ocean sea surface temperatures on Australian region seasonal tropical cyclone counts. J Clim 30:4843–4856

Rayner N, Parker DE, Horton E, Folland CK, Alexander LV, Rowell D, Kent EC, Kaplan A (2003) Global analyses of sea surface temperature, sea ice, and night marine air temperature since the late nineteenth century. J Geophys Res Atmos 108(D14). https://doi.org/10.1029/2002JD002670

Ren HL, Jin FF (2011) Niño indices for two types of ENSO. Geophys Res Lett 38(4). https://doi.org/10.1029/2010GL046031

Risbey JS, Pook MJ, McIntosh PC, Ummenhofer CC, Meyers G (2009) Characteristics and variability of synoptic features associated with cool season rainfall in southeastern Australia. Int J Climatol J R Meteorol Soc 29:1595–1613

Santoso A, Hendon H, Watkins A, Power S, Dommenget D, England MH, Frankcombe L, Holbrook NJ, Holmes R, Hope P (2019) Dynamics and predictability of El Niño-Southern Oscillation: an Australian perspective on progress and challenges. Bull Am Meteor Soc 100:403–420

Takahashi K, Montecinos A, Goubanova K, Dewitte B (2011) ENSO regimes: reinterpreting the canonical and Modoki El Niño. Geophys Res Lett 38(10). https://doi.org/10.1029/2011GL047364

Taschetto A, Ummenhofer C, Sen Gupta A, England M (2009) Effect of anomalous warming in the central Pacific on the Australian monsoon. Geophys Res Lett 36(12). https://doi.org/10.1029/2009GL038416

Timbal B, Drosdowsky W (2013) The relationship between the decline of Southeastern Australian rainfall and the strengthening of the subtropical ridge. Int J Climatol 33:1021–1034

Ummenhofer CC, England MH, McIntosh PC, Meyers GA, Pook MJ, Risbey JS, Gupta AS, Taschetto AS (2009) What causes southeast Australia's worst droughts? Geophys Res Lett 36(4). https://doi.org/10.1029/2008GL036801

van Rensch P, Cai W (2014) Indo-Pacific–induced wave trains during austral autumn and their effect on Australian rainfall. J Clim 27:3208–3221

Wang G, Cai W (2020) Two-year consecutive concurrences of positive Indian Ocean Dipole and Central Pacific El Niño preconditioned the 2019/2020 Australian "black summer" bushfires. Geosci Lett 7:1–9

Wang G, Hendon HH (2007) Sensitivity of Australian rainfall to inter–El Niño variations. J Clim 20:4211–4226

Wang G, Cai W, Yang K, Santoso A, Yamagata T (2020) A unique feature of the 2019 extreme positive Indian Ocean Dipole event. Geophys Res Lett 47:e2020GL088615

Watterson I, O'Kane T, Kitsios V, Chamberlain M (2021) Australian rainfall anomalies and Indo-Pacific driver indices: links and skill in 2-year-long forecasts. J South Hemisphere Earth Syst Sci 71:303–319

Watterson I (2020) Australian rainfall anomalies in 2018–2019 linked to Indo-Pacific driver indices using ERA5 reanalyses. J Geophys Res Atmos 125:e2020JD033041

Weng H, Ashok K, Behera SK, Rao SA, Yamagata T (2007) Impacts of recent El Niño Modoki on dry/wet conditions in the Pacific rim during boreal summer. Clim Dyn 29:113–129

Wittwer G, Waschik R (2021) Estimating the economic impacts of the 2017–2019 drought and 2019–2020 bushfires on regional NSW and the rest of Australia. Aust J Agric Resour Econ 65:918-936. https://doi.org/10.1111/1467-8489.12441

Wittwer G (2020) Estimating the Regional Economic Impacts of the 2017 to 2019 Drought on NSW and the Rest of Australia; Victoria University, Centre of Policy Studies. Budapest, Hungary, IMPACT Centre

Yeh S-W, Kug J-S, Dewitte B, Kwon M-H, Kirtman BP, Jin F-F (2009) El Niño in a changing climate. Nature 461:511–514

Yeh S-W, Kug J-S, An S-I (2014) Recent progress on two types of El Niño: Observations, dynamics, and future changes. Asia-Pac J Atmos Sci 50:69–81

Yuan C, Yamagata T (2015) Impacts of IOD, ENSO and ENSO Modoki on the Australian winter wheat yields in recent decades. Sci Rep 5:1–8

Publisher's Note Springer Nature remains neutral with regard to jurisdictional claims in published maps and institutional affiliations.